Front. Earth Sci. 2021, 15(2): 272–282
https://doi.org/10.1007/s11707-021-0925-6

RESEARCH ARTICLE

Biogenic gas generation effects on anthracite molecular structure and pore structure

Aikuan WANG (✉)[1,2], Pei SHAO[3], Qinghui WANG[1,2]

1 Key Laboratory of Coalbed Methane Resources & Reservoir Formation Process (Ministry of Education), China University of Mining & Technology, Xuzhou 221008, China
2 School of Resources and Geosciences, China University of Mining & Technology, Xuzhou 221116, China
3 Department of Surveying and Planning, Shangqiu Normal University, Shangqiu 476000, China

© Higher Education Press 2021

Abstract This study carries out a simulated experiment of biogenic gas generation and studies the effects of gas generation on the pore structure and molecular structure of anthracite by mercury intrusion porosimetry, X-ray diffraction (XRD) and Fourier transform infrared spectroscopy (FT-IR). The results show that methanogenic bacteria can produce biogenic gas from anthracite. CO_2 and CH_4 are the main components of the generated biogas. After generation, some micropores (<10 nm) and transitional pores (10–100 nm) in the coal samples transform into large pores. In the high-pressure stage (pressure >100 MPa) of the mercury intrusion test, the specific surface area decreases by 19.79% compared with that of raw coal, and the pore volume increases by 7.25% in total. Microbial action on the molecular structure causes changes in the pore reconstruction. The FT-IR data show that the side chains and hydroxyl groups of the coal molecular structure in coal are easily metabolized by methanogenic bacteria and partially oxidized to form carboxylic acids. In addition, based on the XRD data, the aromatic lamellar structure in the coal is changed by microorganisms; it decreases in lateral size (*L*a) and stacking thickness (*L*c). This study enriches the theory of biogenic coalbed gas generation and provides a pathway for enhancing the permeability of high-rank coal reservoirs.

Keywords biogenic gas, anthracite, pore structure, molecular structure

1 Introduction

The Qinshui Basin and the eastern margin of the Ordos Basin are the main commercial development bases of the coalbed methane (CBM) industry in China (Yao et al., 2013; Chen et al., 2018a). Coal reservoirs in China have the characteristics of low gas saturation, low permeability and low pressure; these qualities result in low production in many areas (Liu et al., 2013; Fu et al., 2021). Compared with middle- and low-rank coal, high-rank coal generally has a lower porosity and permeability (Chakhmakhchev 2007; Chen et al., 2018b; Qin et al., 2018). To produce methane successfully, new coal seam permeability enhancing technology is urgently needed.

Biogenic CBM has been found in many coal-bearing basins worldwide (Miyazaki 2005; Warwick et al., 2008; Strąpoć et al., 2011; Yun et al., 2012, Yoon et al., 2016; Fu et al., 2019). Microorganisms can degrade coal organic matter and convert it into biogenic gas through their own metabolic activities when coal reservoirs have a suitable external environment (Green et al., 2008; Jones et al., 2010; Penner et al., 2010; Beckmann et al., 2011; Haider et al., 2013; Gao et al., 2013; Wang and Shao, 2019). Microbial action not only consumes coal organic matter and changes its molecular structure but also changes the coal pore structure and pore connectivity, thus affecting the adsorption, diffusion and migration of CBM (Xia et al., 2014). Jones et al. (2010) proposed that the bioavailability of coal organic matter could be improved by increasing the number of microorganisms and enhancing their activity. Many companies in the United States (Luca Technologies, CirisEnergy and Next Fuel) have reaped significant economic benefits by strengthening microbial activity to increase the production of biogenic gas (Daniel et al., 2015). Apex Australia injects methanobacteria into coal seams in the Sydney Basin to stimulate biogas generation

Received January 15, 2021; accepted June 17, 2021

E-mail: 13815383142@163.com

(Faiz et al., 2013). All these research results provide theoretical and practical support for the feasibility of biological permeability enhancement in coal reservoirs.

This study analyzes the effects of biogenic gas generation on the pore structure and molecular structure of anthracite by comparing the molecular and pore structure changes detected by the mercury injection curve, X-ray diffraction (XRD) and Fourier transform infrared spectroscopy (FTIR) of coal samples before and after the simulated experiment. The research results are helpful for developing a deep understanding of the generation mechanism of biogenic gas from coal and for providing a new way to enhance the permeability of the CBM reservoir.

2 Samples and methods

2.1 Samples

Two samples, No. SH1 and SH2, were collected from the Sihe Coal Mine in the Shanxi Province of China. The samples collected in the mine were immediately wrapped in thin film and sealed in black plastic bags to prevent oxidation. The samples were crushed to 60 mesh, and the pure coal samples were selected manually. Each coal sample was divided into two parts, one for basic property testing and the other for the biogas generation simulation experiment.

The coal samples were subjected to a natural analytic process before the simulated experiment. They were preliminarily crushed first and then put into a flask linked to a beaker with water by a glass catheter. The flask was placed in a constant temperature water bath at 60°C for 7 days. The natural analysis process was considered complete when bubbles were no longer observed in the water. After this test, coal samples were put into an anaerobic incubator (model SYQX-II) to isolate the anaerobic bacteria.

The maximum vitrinite reflectance ($R_{o,max}$) was measured on a Zeiss Imager Mim microscope. Proximate analysis was conducted according to ASTM Standards D3173-11, D3175-11, and D3174-11. The elemental analysis was conducted according to ASTM Standard D5373-08. The maceral composition of coal samples was determined according to national standard GB/T8899-2013 of China. The test results of the basic properties of the sample are shown in Table 1.

The $R_{o,max}$ values of SH1 and SH2 are 2.44% and 2.87%, respectively, which means that the coal samples have high maturity and that the coal rank is in the anthracite stage. The results of proximate analysis show that coal is dominated by fixed carbon, and its content is approximately 80%. The average content of the ash is 10.81%. The average M_{ad} and A_d are 1.63% and 8.50%, respectively, and the carbon content of coal samples is above 90%. The contents of oxygen, hydrogen and nitrogen are all less than 4%. The average content of total sulfur is 0.43%. Only vitrinite and inertinite are present in the organic macerals of the coal. Vitrinite is the main component, accounting for more than 70%, and the average content of inertinite is 19.2%.

2.2 Biogenic gas simulation experiment

The bacterial solution was enriched and purified from mine water from the Dananhu Coal Mine of the Hami coalfield in China, which was supplied by the Chinese Academy of Science. The enrichment culture method was presented in our previous study (Shao et al., 2018). A 500 mL brine bottle with a butyl rubber stopper and wax seal was selected to serve as the simulation experiment device to ensure good airtightness. The assembly of the culture-gas collection device is shown in Fig. 1. It was composed of a culture bottle, a needle, a 3-way valve, a 2-way valve, and a 10 mL screw syringe (Fig. 1). The gas was collected by downward discharge of saturated salt water.

The simulation experiment had six groups. Two groups were blank groups (BK), which acted as controls: No. SH1-BK and SH2-BK. The other four groups were the experimental groups, No. SH1-1, SH1-2, SH2-1, and SH2-2, which means that each coal sample had a parallel group. The coal samples were crushed to approximately 2 mm pieces. Fifty milliliters of the bacterial seed solution and 350 mL of culture solution were added to each of the six groups of experiments. Then, 30 g of each coal sample was added to each of the four experimental groups. The whole inoculation experiment was carried out in a SYQX-II anaerobic incubator. The inoculated saline flask was placed in an HZQ-F160 constant temperature oscillation incubator. The temperature was set to 37°C, and the rotational speed was 50 rad/min.

Table 1 Test data of basic properties of coal samples

Coal samples	$R_{o,max}$/%	Proximate analyses/%				Elemental analyses/%				Maceral composition/%		
		M_{ad}	A_d	V_{daf}	FC_d	O_{daf}	C_{daf}	H_{daf}	N_{daf}	$S_{t,d}$	Vitrinite	Inertinite
SH1	2.44	1.16	12.95	9.84	78.48	3.58	91.27	3.44	1.35	0.31	74.2	20.2
SH2	2.87	2.10	8.66	7.16	84.80	2.01	93.33	2.95	1.10	0.55	79.2	18.3

Notes: $R_{o,max}$ is the maximum vitrinite reflectance; M_{ad} is moisture on an air-dry basis; A_d is Ash on a dry basis; V_{daf} is volatile matter on a dry and ash-free basis; FC_d is fixed carbon content on a dry basis. O, C, H, and N were determined on a dry and ash-free basis, and S was determined on a dry basis.

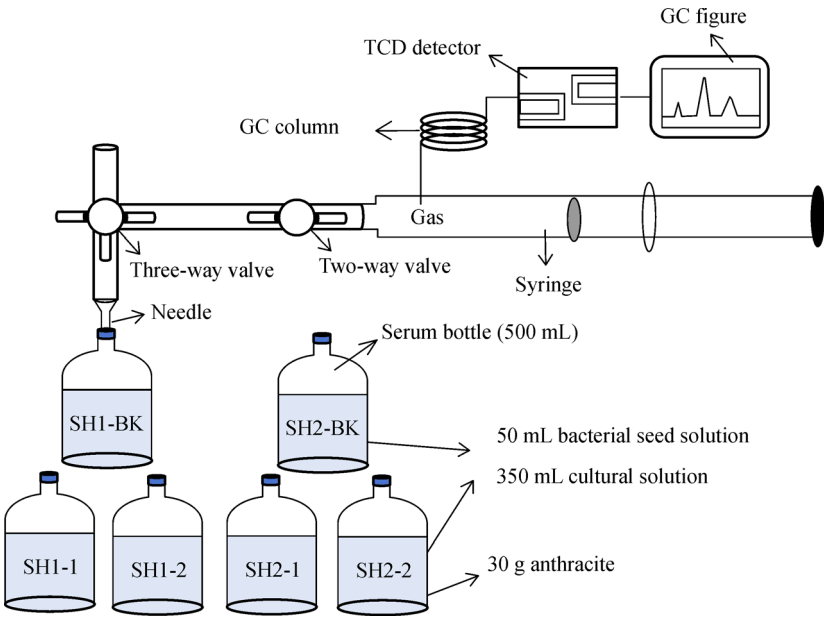

Fig. 1 Schematic diagram of the simulation experiment device.

After 20 days of incubation, the gas was collected and analyzed by gas chromatography (Agilent 7890GC). A thermal conductivity detector (TCD) was used at a detection temperature of 80°C, a chromatographic column temperature of 50°C and a driving gas of 0.5 MPa normal oxygen. The results show that methane gas was produced, which indicates that the simulation experiment was successful.

At the end of the 80-day simulation experiment, the remaining coal samples in each group of culture bottles were removed and placed in an anaerobic incubator SYQX-II to wash clean. After the surface was completely dry, the samples were put into an anaerobic drying oven at a constant temperature of 40°C for 5 h. The samples were divided into three parts for mercury intrusion testing, XRD and FT-IR spectroscopy. The samples were handled in strict accordance with the standard processes and conformed to the requirements of each test.

2.3 Mercury intrusion test

The samples were dried at 70°C–80°C for 12 h in an oven, and then the samples were tested. The instrument was an Auto Pore IV 9510 V1.09 type mercury intrusion microporometer made in the USA. The maximum injection pressure of the instrument was 414 MPa, and the minimum pore size it could measure was approximately 3 nm.

2.4 X-ray diffraction

X-ray diffraction (XRD) is an effective method to analyze the crystal structure of coal. The X-ray diffractometer was a D8 ADVANCE from BRUKER, Germany. The voltage and current of the X-ray tube were 40 kV and 30 mA, respectively. The anode target was Cu target material with Kα radiation. The radius of the goniometer was 250 mm. the Cu-Kβ ray was filtered by an Ni filter. The detector was a LynxEyeTM detector. The diffraction angle (2θ) was 0–80°. The coal samples were crushed to 325 mesh, and 0.5 g of the sample was used for the test.

2.5 Fourier transform infrared (FT-IR) spectroscopy

FT-IR spectroscopy of coal was measured by a BRUKER VERTEX 80v infrared spectrometer. The wavenumber range was 8000–350 cm^{-1} with a resolution of 0.06 cm^{-1}. The peak-to-peak noise was $< 8.6 \times 10^{-6}$Abs. The signal-to-noise ratio was larger than 55000:1 (peak-to-peak). The beam diameter was usually 40 mm, and the Michelson interferometer was calibrated dynamically with high accuracy. The coal samples were crushed to 200 mesh, and a 2.0 g sample was used for the test.

The overall experimental procedure is shown in Fig. 2.

3 Results

3.1 Results of the gas production

Table 2 lists the gas production and the contents of CO_2 and CH_4 from biogas on days 20, 40, 60, and 80. Because the amount of gas generated on the 60th day was relatively low, the gas composition was not measured on that day. SH1-BK and SH2-BK no longer produced gas at 60 days and 80 days, respectively, indicating that the nutrient solution had been completely metabolized by microorgan-

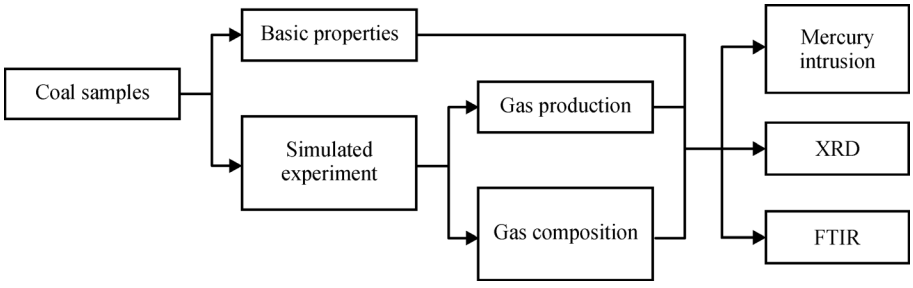

Fig. 2 The overall experimental procedure of the study.

Table 2 Production and contents of biogas during different stages

Samples	20 d			40 d			60 d	80 d		
	Gas production /mL	CO_2 content /%	CH_4 content /%	Gas production /mL	CO_2 content /%	CH_4 content /%	Gas production /mL	Gas production /mL	CO_2 content /%	CH_4 content /%
SH1-BK	22.8	62.61	37.29	11.2	14.98	85.02	0	0	0.00	0.00
SH1-1	63.4	55.20	44.80	27.5	32.19	67.81	13.2	7.3	3.56	96.44
SH1-2	66	84.28	15.72	23.5	27.46	72.54	18.6	12.5	4.22	95.78
SH2-BK	20.6	51.83	48.07	13.5	15.87	84.13	0	0	0.00	0.00
SH2-1	79.8	68.39	31.61	29.1	22.82	77.18	15.4	13.7	4.02	95.98
SH2-2	71	47.91	52.09	24.6	21.80	78.20	16.7	10.4	3.98	96.02

isms. Subsequently, biogas was still generated in the experimental groups, which meant that in this study, anthracite could generate biogas. The difference in the gas production of the experimental groups and the blank groups was considered the gas production of the anthracite sample under the action of methanogens, which can be seen in Fig. 3(a). Gas production peaked at 20 days and then decreased and reached a plateau at 40 days. At the end of the experiment, the average total gas productions of SH1 and SH2 were 82 mL and 94.5 mL, respectively. The biogas production rates were 2.673.15 mL/g and 3.15 mL/g, respectively.

The GC test results showed that CH_4 and CO_2 were the main components of the simulated biogas produced from all the groups. In the first 20 days, much CO_2 was produced, and then its concentration decreased, while the CH_4 changes showed the opposite trend (Fig. 3(b)). At present, it is concluded that there are two pathways to produce biomethane, namely, acetic acid fermentation and CO_2 reduction (Opara et al., 2012; Wang et al., 2017). The complementary relationship between CO_2 and CH_4 suggests that CH_4 was partly produced via CO_2 reduction in this simulated experiment; this conclusion is consistent with those of previous studies (Wang and Shao, 2019).

3.2 Results of mercury intrusion test

Figure 4 shows the mercury intrusion and extrusion curves of the raw coal samples and coal samples after biogenic gas generation. SH1-BK and SH2-BK are the raw coal samples. SH1-1, SH1-2, SH2-1, and SH2-2 are the parallel samples under the biogenic gas generation experiment. The ordinate in Fig. 4 indicates the ratio of the cumulative Hg intake during that stage to the maximum Hg intake in units of %. As shown in Fig. 4, in the high pressure stage (pressure $>$ 100 MPa), the mercury saturation increases rapidly with increasing pressure, which means that there are more small pores in the coal samples. In addition, the intrusion-extrusion hysteresis loops of the samples treated in the biogenic gas generation experiment (SH-1, SH1-2, SH2-1, and SH2-2) are obviously larger than those of raw coal (SH1-KB and SH2-KB). This result is likely caused by methanogen activity.

3.3 XRD test results

There are two peaks in the XRD pattern of coal, which indicate its molecular structure. The (002) plane diffraction peaks between 10° and 35° reflect the stacking height of the aromatic layers, and the (100) plane diffraction peaks between 35° and 50° reflect the condensation degree of the aromatic rings.

Figure 5 shows the XRD patterns of the raw coal samples and the coal samples after biogenic gas generation. SH1-BK and SH2-BK are raw coal samples, and SH1-1, SH1-2, SH2-1 and SH2-2 are experimental samples after biogenic gas generation. After biodegradation, the XRD patterns of SH1 and SH2 are consistent with those of raw coal. However, the peak heights of the experimental groups are reduced, especially in the range of

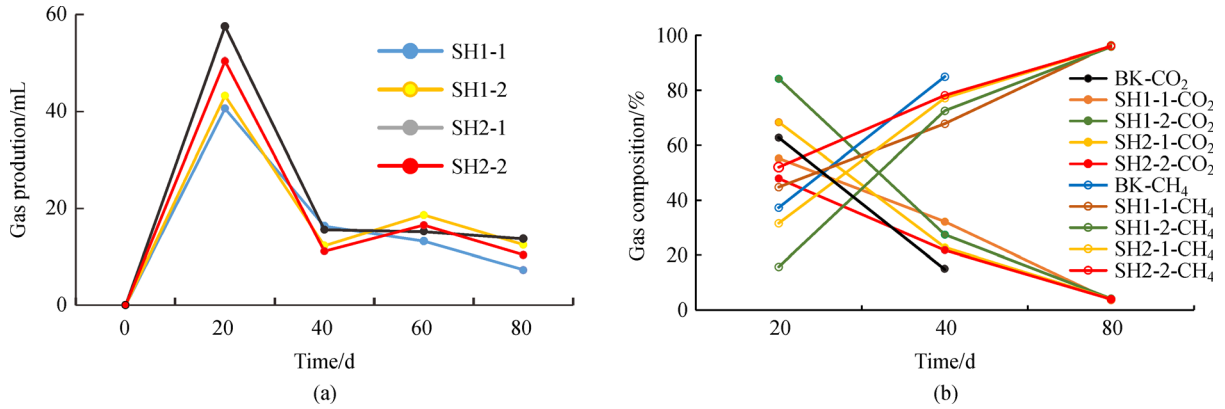

Fig. 3 The changes in the simulated gas production and gas composition during the experiment. (a) Change in the production of biogas of the anthracite samples; (b) change in gas compositions of all groups.

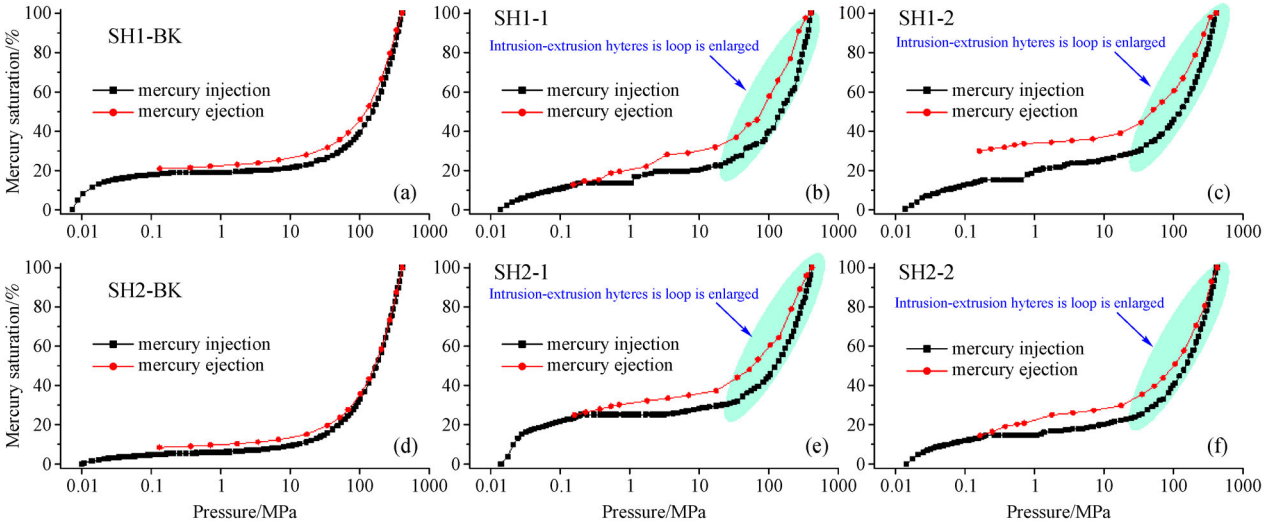

Fig. 4 Mercury intrusion and extrusion curves of the samples.

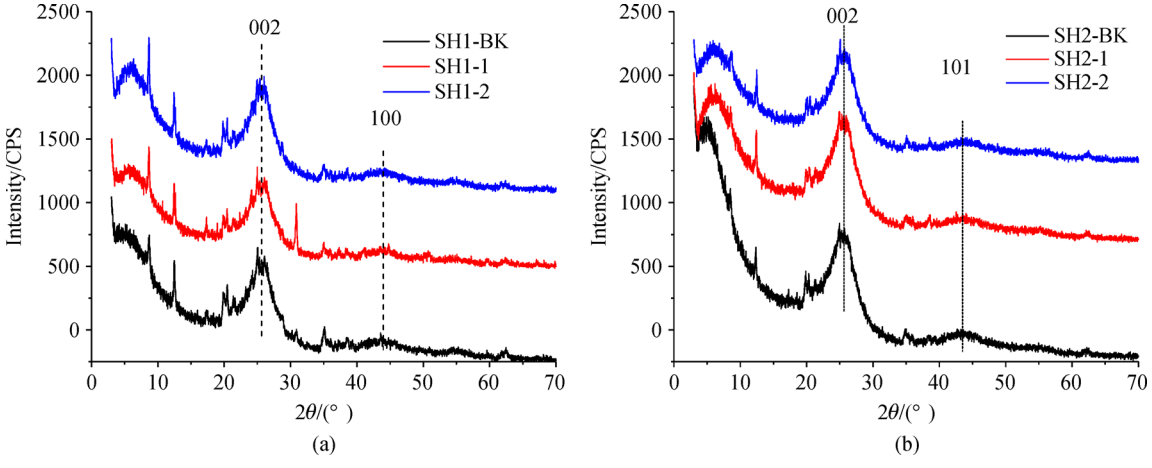

Fig. 5 XRD patterns of coal samples. (a) Raw coal samples; (b) after biogenic gas generation.

10°–30°, while the reduction in the range of 35°–50° is slightly weaker. This result indicates that biodegradation can effectively degrade the aromatic layer thickness and the condensation degree of aromatic rings in the chemical structure of anthracite. For all the XRD spectra, there are two main peaks located at 20°–30° and 40°–50°, and it can also be seen that there is a small amount of minerals in these six samples.

3.4 FT-IR spectroscopy results

Figure 6 shows the FT-IR spectra of raw coal and the coal samples after gas generation. SH1-BK and SH2-BK are raw coal samples, and SH1-1, SH1-2, SH2-1, and SH2-2 are experimental samples after biogenic gas generation. According to the theory of infrared spectroscopy and organic chemistry, there are four main kinds of absorption peaks in the infrared spectrum (Fig. 6): characteristic absorption peaks of aromatic hydrocarbon structures (700–900 cm^{-1}), characteristic absorption peaks of heteroatom functional groups containing oxygen (1000–1800 cm^{-1}), and characteristic absorption peaks of aliphatic structures (2800–3000 cm^{-1}), (3000–3600 cm^{-1}), which are the characteristic absorption peaks of hydroxyl structures.

The infrared spectra of the raw coal and biodegraded coal samples have typical characteristic peaks. In the spectra, there are strong and wide bands in the 3000–3600 cm^{-1} range, which are mainly-OH stretching vibration absorption peaks from the coal molecular structure. The 2800–3000 cm^{-1} range has no obvious

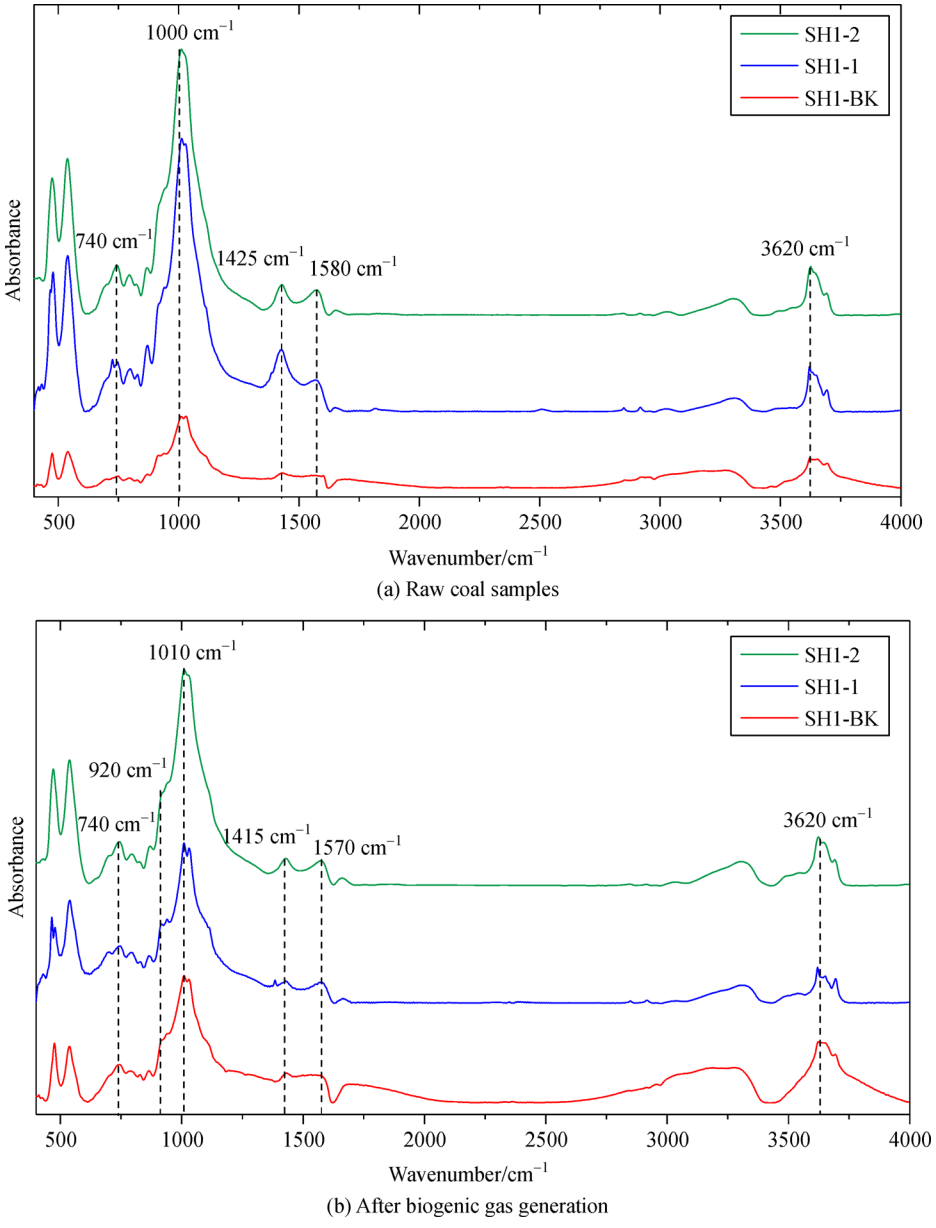

Fig. 6 Infrared spectrogram of coal samples.

absorption peaks. In the spectral ranges of 1000–1800 cm^{-1} and 700–900 cm^{-1}, there are mainly aromatic hydrocarbons and oxygen-containing functional groups, and the distribution of aromatic structures is relatively high, indicating that the maturity of the coal is relatively high. The FTIR spectra of the samples after biodegradation show that the corresponding bands of aromatic structure increased and widened, and the peaks in the 3000–3600 cm^{-1} range flattened, indicating that the-OH structure was weakened.

4 Discussion

4.1 Effect of biogenic gas generation on the pore structure of coal

Based on the interactions between pores and gas molecules (Li et al., 1999), the pore size of coal in this research was divided into four categories: macropores (> 1000 nm), mesopores (100–1000 nm), transition pores (10–100 nm) and micropores (< 10 nm). The pore volume and specific surface area of each pore section of the coal sample were calculated based on the mercury injection test results, as shown in Table 3. The relationships between the mercury stage intrusion amount and pore size are shown in Fig. 7.

In Table 3 and Fig. 7, it can be seen that the total pore volume of each coal sample increases and the total specific surface area decreases after biomethanation, which indicates that the pore structure of coal can be modified by biomethanation. The pore volumes and specific surface areas of the micropores and transition pores are reduced by 19.79% on average, while the pore volumes and specific surface areas of the mesopores and macropores are increased by 7.25% on average. For example, after methanogenesis, the pore volume of sample SH2 decreased from 0.021 cm^3/g to 0.019 cm^3/g and 0.018 cm^3/g, the pore specific surface area decreased from 19.923 m^2/g to 15.812 m^2/g and 15.626 m^2/g, while the mesopore volume increased from 0.001 cm^3/g to 0.002 cm^3/g and 0.001 cm^3/g, and the pore specific surface area increased from 0.027 m^2/g to 0.033 m^2/g and 0.029 m^2/g. Micropores have a large specific surface area and can provide enough living space for microorganisms. The metabolic activities of microorganisms consume the coal organic matter around the pores, reducing the number of original micropores and transition pores and increasing the pore volume to form mesopores or even macropores, which results in a higher contribution to pore volume and specific surface area by larger pores.

The mercury intrusion and extrusion curve (Fig. 4) shows that the mercury intrusion and withdrawal curve of the BK group is basically closed. When the mercury intrusion pressure is equal to the mercury withdrawal pressure, the mercury saturation in the pores is basically equal, indicating that the pores in the coal are mainly semiclosed pores and that there are fewer open pores. The distance between the two loops is similar, indicating that the pores are relatively isolated and have poor connectivity. After biomethanogenesis, the curves of the mercury advance and retreat in the SH1 and SH2 groups were distant, and the hysteresis loops became larger, which indicated that the interpore connectivity was enhanced and the number of open pores also increased, which may be the result of the abovementioned microbial modification of pore size distribution.

4.2 Effect of biogenic gas generation on the molecular structure of coal

Origin 7.5 software was used to fit the X-ray diffraction pattern, and the peak width at half maximum and 2θ of the (002) plane diffraction peak and (100) plane diffraction peak were obtained. Bragg's law (Eq. (1)) and the Scherrer formula (Eq. (2) and Eq. (3)) were used to calculate the microcrystalline structure parameters of the samples (the aromatic interlayer distance d_{002}, aromatic ring layer thickness Lc and aromatic layer ductility La). The results are shown in Table 4.

$$d_{002} = \frac{\lambda}{2\sin\theta_{002}}, \tag{1}$$

$$Lc = \frac{k_1\lambda}{\beta_{002}\cos\theta_{002}}, \tag{2}$$

Table 3 The pore volume and specific surface area distributions of each pore segment of the samples

Samples	Total pore volume /($cm^3 \cdot g^{-1}$)	Pore volume distribution/%				Total specific surface area / ($m^2 \cdot g^{-1}$)	Specific surface area distribution/%			
		Macropores	Mesopores	Transitional pores	Micropores		Macropores	Mesopores	Transitional pores	Micropores
SH1-BK	0.031	6.45	3.23	25.81	64.52	20.071	0.00	0.10	8.48	91.41
SH1-1	0.032	15.63	3.13	21.88	59.38	17.562	0.03	0.10	7.25	92.63
SH1-2	0.031	19.35	6.45	22.58	51.61	15.178	0.03	0.19	9.61	90.16
SH2-BK	0.031	3.23	3.23	25.81	67.74	22.063	0.00	0.12	9.57	90.30
SH2-1	0.034	14.71	5.88	23.53	55.88	17.552	0.01	0.19	9.72	90.09
SH2-2	0.036	25.00	2.78	19.44	50.00	17.244	0.01	0.17	9.21	90.62

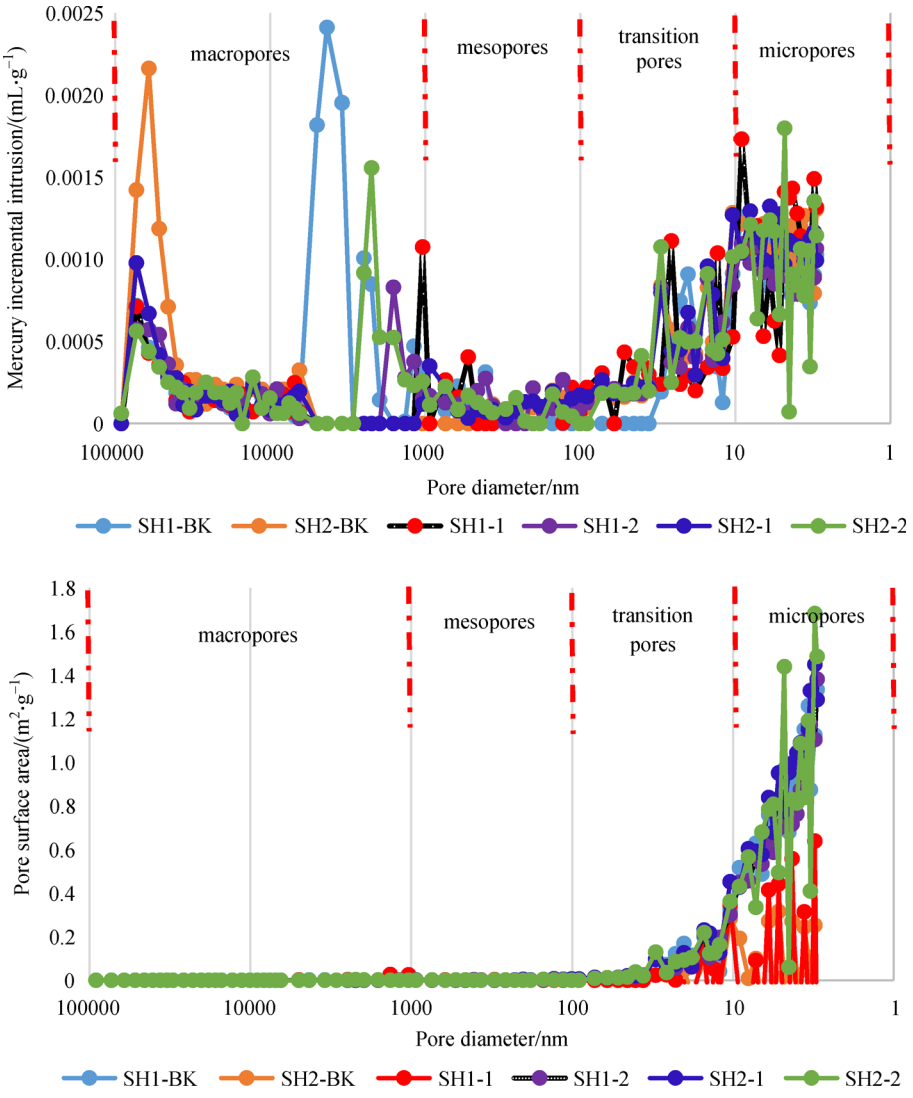

Fig. 7 Relation diagrams of stage mercury intrusion (a) and stage pore area (b) with pore diameters of raw and experimental coal samples after biodegradation.

$$La = \frac{k_2 \lambda}{\beta_{100} \cos\theta_{100}}, \tag{3}$$

where λ is the wavelength of the X-ray, 1.5406 Å; β_{002} and β_{100} are the half-peak widths of the (002) plane diffraction peak and (100) plane diffraction peak, rad; θ_{002} and θ_{101} are the Bragg angle of the (002) plane diffraction peak and (100) plane diffraction peak, rad.

As shown in Table 4, the spacing (d_{002}) between the aromatic ring layers of the SH1 and SH2 coal samples after biomethanation remained stable, but the stacking thickness (Lc) decreased, with that of the SH2 samples decreasing from 19.61 Å to 18.92 Å and 18.54 Å, and the effective number of stacking layers (Lc/d_{002}) of the aromatic ring laminates was also reduced accordingly. The elongation (La) of the aromatic layer sheet also decreased, and that of the SH2 samples changed from 23.01 Å to 21.82 Å and 22.15 Å. The results show that the whole lattice structure of the samples was stable overall, but some branched chain structures changed. Under the influence of biological metabolism, the aromatic molecule structure in the coal sample degraded, and the aromatic bonds opened to form chain-like molecules, which led to the weakening of the orientation arrangement and the decreasing crystallization degree of the aromatic layer. The effect of the biogenic gas metabolism pore structure of the coal in a study by Xia et al., (2014) shows that the stacking degree and ductility of the aromatic layers decreased, but the spacing of aromatic carbon layers increased. The former is consistent with the research results of this paper, and the inconsistent results of the latter may be caused by the degree of maturity of the coal sample. The coal samples studied in this report were anthracite with $R_{o,max}$ values higher than 2.0%, and coal samples used by Xia et al. (2014) were less mature

Table 4 Peak fitting results of XRD peak parameters of coal samples

Coal samples	(002) Plane diffraction peak			(100) Plane diffraction peak			Coal structure parameters			
	2θ/(°)	θ/rad	β_{002}/rad	2θ/(°)	θ/rad	β_{100}/rad	d_{002}/Å	Lc/Å	La/Å	Lc/d_{002}
SH1-BK	25.46	0.22	0.08	42.22	0.37	0.14	3.5	19.52	22.27	5.58
SH1-1	25.44	0.22	0.08	44.15	0.39	0.14	3.5	19.25	21.82	5.5
SH1-2	25.67	0.22	0.08	44.04	0.38	0.14	3.47	19.11	21.63	5.51
SH2-BK	25.19	0.22	0.08	43.82	0.38	0.13	3.53	19.61	23.01	5.55
SH2-1	25.74	0.22	0.08	43.84	0.38	0.14	3.46	18.92	21.82	5.47
SH2-2	25.81	0.23	0.08	43.84	0.38	0.14	3.45	18.54	22.15	5.38

with $R_{o,max}$ values of 0.56%–1.51%. The crystal structure of the coal with high maturity is more stable (Liu et al., 2018), so the whole lattice structure exerted a lesser influence.

4.3 Effect of biogenic gas generation on coal structure

Origin 7.5 software was used to fit the four parts of the infrared spectrogram, and the results were normalized. According to previous research results, different peak positions were assigned, the relative contents of different functional groups were determined, and finally, the coal structure parameters were calculated (Zheng et al., 2011; Xia et al., 2014). The results are shown in Table 5.

There are five main types of structural parameters. Parameter I1 denotes the degree of aliphatic chain branching and is numerically characterized by the ratio of the absorption peak areas in the range of 2940–2900 cm^{-1} and 3000–2940 cm^{-1} (Ibarra et al., 1994); 2940–2900 cm^{-1} is mainly the straight chain part ($-CH_2$) of the aliphatic chain, aliphatic ring and aromatic side chain, and 3000–2940 cm^{-1} is mainly the branched chain part ($-CH_3$) of the aliphatic side chain. Parameter I2 denotes the degree of hydrogen enrichment and is numerically characterized by the ratio of absorption peak areas of 3000–2800 cm^{-1} and 1600–1500 cm^{-1}; 3000–2800 cm^{-1} is mainly the stretching vibration of methyl and methylene, and 1600–1500 cm^{-1} is mainly the C = C skeleton vibration of aromatic hydrocarbons. Parameter I3 denotes the degree of aromatization and is numerically characterized by the absorption peak area ratios in the ranges of 3100–3000 cm^{-1} and 3000–2800 cm^{-1} (Guo and Bustin, 1998). Peaks in the range of 3100–3000 cm^{-1} are mainly due to the stretching vibrations of aromatic hydrocarbon C-H bonds. Parameters I4 and I5 represent the abundance of hydroxyl and carboxyl groups in coal, respectively (Xia et al., 2014). As shown in Table 5, after biomethanation, the length of aliphatic chains in the coal decreases and the degree of hydrogen enrichment decreases, indicating that microbial metabolism disconnects the branched and side chains of aliphatic hydrocarbons and aromatic hydrocarbons, and the hydroxyl groups in the coal are also consumed. Methyl ($-CH_3$) and methylene ($-CH_2$) groups in coal are oxidized to form carboxyl groups, so the number of carboxyl groups is relatively increased. The results are consistent with the acetic acid fermentation methanogenic pathway of microorganisms. The degree of aromatization decreased slightly, indicating that microbial action could break up the aromatic structure, which was consistent with the XRD analysis results.

The overall effect of biogenic coalbed gas production on the pore characteristics and chemical structure of anthracite is shown in Fig. 8. Biological metabolism can transform coal pores, reduce the number of micropores and transition pores, and reduce the specific surface area of the pores. The increase in large pores leads to an increase in the overall pore volume, the transformation of semi-open pores to open pores, an increase in pore connectivity, which is conducive to gas desorption in coal seams, and the acceleration of the migration and production of coalbed gas. The modification of coal pores by methanogenic bacteria is due to the metabolic activity of microorganisms. Microorganisms adhering to the surfaces of micropores and transitional pores utilize the surrounding organic matter to produce biogas, in which methyl and methylene groups and hydroxyl groups in the aliphatic chains and

Table 5 FI-IR parameters and their meanings of coal structure

Parameters	Meaning	Numerical Representation	Samples		
			SH1-BK	SH1-1	SH1-2
I1	Branched chain of fat	A(2940–2900 cm^{-1})/A(3000–2940 cm^{-1})	3.70	1.97	1.97
I2	Hydrogen-enriched degree	A(3000–2800 cm^{-1})/A(1800–1500 cm^{-1})	0.91	0.16	0.05
I3	aromatization	A(3100–3000 cm^{-1})/A(3000–2800 cm^{-1})	1.92	1.03	1.44
I4	Hydroxyl expansion vibration	A(3600–3000 cm^{-1})	1.97	0.89	1.14
I5	Carboxyl expansion vibration	A(1500–1350 cm^{-1})	0.32	1.01	0.55

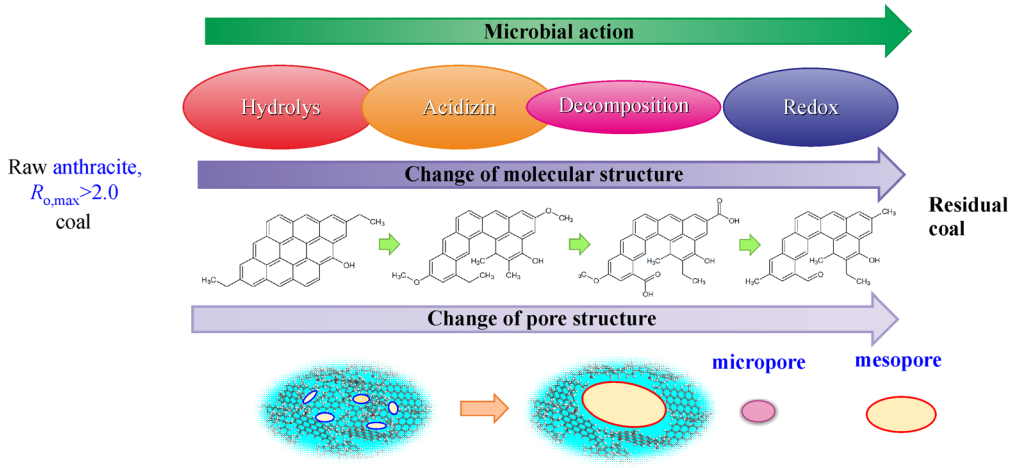

Fig. 8 Schematic diagram of the effect of biogenic coalbed gas generation on anthracite pore structure and molecular structure.

aromatic side chains of coal are consumed, and methyl and methylene groups are fermented by microorganisms to form carboxyl groups, which are eventually converted into biogas. The aromatic structure of the coal is also destroyed, and the aromatic ring is opened, which reduces the aromatization degree of the coal.

5 Conclusions

The experiments confirmed that anthracite can be utilized by methanogenic bacteria as the substrate to produce biogas. In this 80-day experiment, anthracite had large biological potential, as reflected by the gas production (82 mL and 94.5 mL) and generation rates (2.67 mL/g and 3.15 mL/g). CO_2 and CH_4 were the main components of the biogas in this study, and their trends showed that CH_4 was partly generated from the CO_2-reduction pathway.

Biogas generation can change the pore structure of anthracite. After biogenic gas generation, the total pore volume of the coal sample increases by 7.25%, on average, and the total specific surface area decreases by an average of 19.79%. The mercury intrusion and extrusion curves show that after the production of biogenic methane, the mercury saturation of coal samples increases rapidly with increasing pressure, especially in the high pressure stage (pressure > 100 MPa), which indicates that there are more small holes and open pores in coal samples, leading to an increase in the inter-void connectivity of the coal.

Biodegradation changes the molecular structure, which leads to a change in the pore structure of the anthracite. The XRD results show that, unlike those of the raw coal samples, the aromatic ring layer spacing (d_{002}) of the experimental coal samples is relatively stable. Biodegradation decreases the single stack thickness Lc and the aromatic layer extension La. This means that the overall lattice structure of the coal samples remains stable, but the molecular structure of the coal changes. FT-IR results show that after biogenic gas production, the length of the aliphatic chain (I1) in coal decreases, the degree of hydrogen enrichment (I2) decreases, the hydroxyl group (I4) in coal is consumed, and the number of carboxyl groups (I5) increases. The aromatization degree (I3) of the coal sample is reduced. The production of biogenic gas changes the aromatic structure of coal, and the ring bonds of aromatic molecules open to reduce the crystallization degree of the coal and create chain-like molecular structures.

Acknowledgements This study was supported by the Fundamental Research Funds for the Central Universities (No. 2019QNA33). The authors would like to thank the anonymous reviewers for their constructive and careful comments on the manuscript.

References

Beckmann S, Krüger M, Engelen B, Gorbushina A A, Cypionka H (2011). Role of *Bacteria*, *Archaea* and *Fungi* involved in methane release in abandoned coalmines. Geomicrobiol J, 28(4): 347–358

Chakhmakhchev A (2007). Worldwide coalbed methane overview, In: SPE hydrocarbon Economics and Evaluation Symposium, SPE. Soc Petrol Eng, 17–23

Chen S, Tang D, Tao S, Xu H, Li S, Zhao J, Cui Y, Li Z (2018a). Characteristics of *in-situ* stress distribution and its significance on the coalbed methane (CBM) development in Fanzhuang-Zhengzhuang Block, Southern Qinshui Basin, China. J Petrol Sci Eng, 161: 108–120

Chen Y L, Qin Y, Wei C T, Huang L L, Shi Q M, Wu C F, Zhang X Y (2018b). Porosity changes in progressively pulverized anthracite subsamples: implications for the study of closed pore distribution in coals. Fuel, 225: 612–622

Ritter D, Vinson DBarnhart E, Akob D, Fields M, Cunningham F, Orem W, McIntosh J (2015). Enhanced microbial coalbed methane

generation: a review of research, commercial activity, and remaining challenges. Int J Coal Geol, 146: 28–41

Faiz M, Stalker L, Sherwood N, Saghafi A, Wold M, Barclay S, Choudhury J, Barker W, Wang I (2003). Bio-enhancement of coal bed methane resources in the southern Sydney Basin. APPEA J, 43(1): 595–610

Fu X H, Zhang X D, Wei C T (2021). Review of research on testing, simulation and prediction of coal bed methane content. J China U Min Techn, 50(1): 13–31 (in Chinese)

Fu H, Yan D, Yang S, Wang X, Zhang Z, Sun M (2020). Characteristics of *in situ* stress and its influence on coalbed methane development: a case study in the eastern part of the southern Junggar Basin, NW China. Energy Sci Eng, 8(2): 515–529

Gao L, Brassell S C, Mastalerz M, Schimmelmann A (2013). Microbial degradation of sedimentary organic matter associated with shale gas and coalbed methane in eastern Illinois Basin (Indiana), USA. Int J Coal Geol, 107: 152–164

Green M S, Flanegan K C, Gilcrease P C (2008). Characterization of a methanogenic consortium enriched from a coalbed methane well in the Powder River Basin, USA. Int J Coal Geol, 76(1–2): 34–45

Guo Y T, Bustin M R (1998). Micro-FTIR spectroscopy of liptinite macerals in coal. Int J Coal Geol, 36(3–4): 259–275

Haider R, Ghauri M A, SanFilipo J R, Jones E J, Orem W H, Tatu C A, Akhtar K, Akhtar N (2013). Fungal degradation of coal as a pretreatment for methane production. Fuel, 104: 717–725

Ibarra J V, Moliner R, Bonet A J (1994). FT-IR investigation on char formation during the early stages of coal pyrolysis. Fuel, 73(6): 918–924

Jones E J P, Voytek M A, Corum M D, Orem W H (2010). Stimulation of methane generation from nonproductive coal by addition of nutrients or a microbial consortium. Appl Environ Microbiol, 76(21): 7013–7022

Li Y H, Lu G Q, Rudolph V (1999). Compressibility and fractal dimension of fine coal particles in relation to pore structure characterisation using mercury porosimetry. Part Part Syst Charact, 16(1): 25–31

Liu A H, Fu X H, Luo B, Luo P, Jiao C (2013). Comprehensive analysis of CBM recovery inLhigh rank coal reservoir of Jincheng area. Int J Min Sci Technol, 23(3): 447–452

Liu Y, Zhu Y, Liu S, Chen S, Li W, Wang Y (2018). Molecular structure controls on micropore evolution in coal vitrinite during coalification. Int J Coal Geol, 199: 19–30

Miyazaki S (2005). Coalbed methane growing rapidly as Australia gas supply diversifies. Oil Gas J, 103(28): 32–36

Opara A, Adams D J, Free M L, McLennan J, Hamilton J (2012). Microbial production of methane and carbon dioxide from lignite, bituminous coal, and coal waste materials. Int J Coal Geol, 96–97: 1–8

Penner T J, Foght J M, Budwill K (2010). Microbial diversity of western Canadian subsurface coal beds and methanogenic coal enrichment cultures. Int J Coal Geol, 82(1–2): 81–93

Qin Y, Moore T A, Shen J, Yang Z B, Shen Y L, Wang G (2018). Resources and geology of coalbed methane in China: a review. Int Geol Rev, 60(5–6): 777–812

Shao P, Wang A, Wang W F (2018). Experimental simulation of biogenic coalbed gas generation from lignite and high-volatile bituminous coals. Fuel, 219: 111–119

Strąpoć D, Mastalerz M, Dawson K, Macalady J, Callaghan A V, Wawrik B, Turich C, Ashby M (2011). Biogeochemistry of microbial coal-bed methane. Annu Rev Earth Planet Sci, 39(1): 617–656

Wang A K, Shao P (2019). Generation processes and geochemical analysis of simulated biogenic coalbed methane from lignite. Geochem Int, 57(12): 1295–1305

Wang B, Tai C, Wu L, Chen L, Liu J, Hu B, Song D (2017). Methane production from lignite through the combined effects of exogenous aerobic and anaerobic microflora. Int J Coal Geol, 173: 84–93

Warwick P D, Breland F C Jr, Hackley P C (2008). Biogenic origin of coalbed gas in the northern Gulf of Mexico Coastal Plain, USA. Int J Coal Geol, 76(1–2): 119–137

Xia D P, Guo H Y, Ma J Q, Si Q, Su X B (2014). Impact of biogenic methane metabolism on pore structure of coals. Nat Gas Geosci, 25(07): 1097–1102 (in Chinese)

Yao Y, Liu D, Qiu Y (2013). Variable gas content, saturation, and accumulation characteristics of Weibei coalbed methane pilot-production field in the southeastern Ordos Basin, China. AAPG Bull, 97(8): 1371–1393

Yoon S P, Jeon J Y, Lim H S (2016). Stimulation of biogenic methane generation from lignite through supplying an external substrate. Int J Coal Geol, 162: 39–44

Yun J, Xu F Y, Liu L, Zhong N N, Wu X B (2012). New progress and future prospects of CBM exploration and development in China. Int J Min Sci Technol, 22(3): 363–369

Zheng Q R, Zeng F G, Zhang S T (2011). FT-IR study on structure evolution of middle maturate coals. Journal of China Coal Society, 36(03): 481–486 (in Chinese)